

THE INTERACTION MECHANISM OF A GLIDING DISLOCATION WITH A STACKING FAULT TETRAHEDRON—H.-J. Lee and B. D. Wirth (University of California, Berkeley)

OBJECTIVE

The objective of this work is to understand the sequence of events controlling the interaction between a stacking fault tetrahedron and gliding edge, screw and 60 degree mixed dislocation using molecular dynamics simulations.

SUMMARY

Interaction mechanisms between stacking fault tetrahedra (SFT) and gliding screw, edge and mixed dislocations are studied using molecular dynamics simulations. For the interaction geometries investigated in this study, different reactions are observed upon contact of the gliding dislocation and an SFT, depending on dislocation character.

1. A screw dislocation constricts and cross-slips on the inclined face of the SFT, partially absorbing the SFT.
2. An edge dislocation induces a reversible instability and partial collapse of the SFT by the inverse Silcox-Hirsch mechanism.
3. A mixed dislocation dissociates into a stair rod partial and Shockley partial dislocations on the inclined face of the SFT.

However, independent of the dislocation character, the trailing partial ultimately detaches from the SFT by an Orowan-like mechanism indicating that an SFT is a strong obstacle to dislocation motion. Following dislocation passage, the resulting defect cluster consists of a smaller perfect SFT and a truncated base, which later forms a sheared SFT with the anticipated extrinsic and intrinsic ledges. The SFT–dislocation interactions are analyzed in terms of the governing partial dislocation reactions.

PROGRESS AND STATUS

Introduction

It is well established that high energy particle irradiation leads to a change in mechanical behavior of materials [1]. For low-to-intermediate temperature irradiation, the characteristic changes include a yield stress increase and ductility decrease. For face centered cubic (FCC) metals like Cu, the yield stress increase is attributed to the production of a high number of irradiation-induced defect clusters in the form of stacking fault tetraheda (SFT). The SFT act as obstacles to dislocation motion, thus changing the local constitutive properties, observed as increases in yield stress and decreases in ductility.

However, the underlying mechanisms responsible for the ductility decreases in irradiated materials is still largely unresolved. TEM examinations of irradiated materials prior to and following deformation reveal the formation of defect free channels, which appear as a cleared band with a very low visible defect density [2]. Early models proposed that a single dislocation interaction with the radiation obstacle led to sweeping or annihilation, producing decreased resistance for subsequent dislocation glide. The defect removal mechanisms are believed to include: (i) drag of mobile defects like interstitial loops via elastic interactions or absorption into a dislocation core, (ii) transformation of the defect cluster to those with reduced resistance, and (iii) shearing of the defects to an invisible small size [3].

In Cu, about 90% of the observed radiation defects are SFTs [4], which likely form directly within displacement cascades, or shortly thereafter, by a Silcox-Hirsch mechanism [5–7]. Generally, the observed radiation defect sizes vary depending on the radiation type, dose and temperature. However, in

neutron as well as ion - irradiated Cu, the average SFT size is 2.5 ± 0.5 nm over a fairly wide irradiation temperature regime of $20 \sim 200^\circ\text{C}$ [8]. Given the uncertainties on the controlling mechanisms of (defect free) channel formation, molecular dynamics (MD) simulation methods can provide understanding of the interaction between the SFT and dislocations, which govern (defect free) channel formation, irradiation hardening and ductility loss.

Previous MD simulations have been used to understand the interaction between an SFT and an edge dislocation in Cu and shown that the SFT is neither absorbed nor destroyed by the interaction [9,10]. Upon further interactions with the edge dislocation, the SFT is sheared further and separated into two pieces, a smaller perfect SFT and a truncated base. Osetsky et al. reported that the critical resolved shear stress (CRSS) increases as the glide plane of an edge dislocation gets closer to the base of the SFT and the temperature decreases [10]. These results are in qualitative agreement with in situ-TEM observations [11].

A screw dislocation is presumed more effective at annihilating SFTs, due to its ability to cross-slip and remove the stacking faults, as initially proposed by Kimura and Maddin [12]. Indeed, early in-situ TEM observations by Johnson et al. [13] and more recently by Robach et al. [11] show that screw dislocations are more efficient than edge dislocations at removing radiation obstacles. Additionally, Matsukawa et al. has reported the annihilation of an SFT base portion by a moving dislocation in in-situ TEM experiments of quenched gold [14].

However, the atomistic details of the interaction between dislocations and SFT are not fully known. In this report, we present the results of MD simulations, which investigate the interactions between SFT and a moving screw, edge and mixed dislocation and the detailed interpretation of simulation results.

Simulation Methods

The MD simulations were performed using the MDCASK code [15] with an embedded atom method (EAM) potential by Mishin and co-workers [16]. The material properties obtained from the Cu EAM potential are summarized in Table 1. Note that the stacking fault energy obtained with this EAM potential (44.4 mJ/m^2) is very close to the experimental value of 45 mJ/m^2 . A realistic stacking fault energy is important because this property controls the width of Shockley partial dislocation separation, as well as SFT stability.

Table 1. The physical properties of Cu

	Experiment [17–18]	EAM [16]
$\alpha [\text{\AA}]$	3.615	3.615
$E_{\text{coh}} [\text{eV}]$	3.54	3.54
B [GPa]	138.3	138.3
C_{11} [GPa]	170.0	169.9
C_{12} [GPa]	122.5	122.6
C_{44} [GPa]	75.8	76.2
γ_{SF} [mJ/m^2]	45	44.4

The comparison between the experimental data and the values obtained from the EAM used in this work [16–18]. Here, the lattice constant α , cohesive energy E_{coh} , bulk modulus B, elastic constants C_{ij} , and stacking fault energy γ_{SF} are shown.

A simulation cell with FCC crystalline structure in orientations of $x = [\bar{1}\bar{1}1]$, $y = 1/2[110]$ and $z = 1/2[1\bar{1}2]$ is used. For a screw dislocation, a simulation cell with 31.4 nm in x, 22.5 nm in y and 44.3 nm in z direction, which is $(50 \times 88 \times 100)$ in unit cells and contains 2.6×10^6 atoms is used. For an edge dislocation, a simulation cell with 31.4 nm in x, 25.5 nm in y and 39.0 nm in z direction, which is $(50 \times 100 \times 88)$ in unit cells and contains 2.6×10^6 atoms is used. For a mixed dislocation, a simulation cell with 12.5 nm in x, 22.5 nm in y and 35.3 nm in z direction, which is $(20 \times 88 \times 80)$ in unit cells and contains \sim

0.84×10^6 atoms is used. Thus, the dislocation line length and inter-particle (SFT) spacing is 22.5 nm for a screw and a mixed dislocation, while 39.0 nm for an edge dislocation.

The screw dislocation of burger's vector (b) $1/2[\bar{1}\bar{1}0]$ is introduced using the elastic isotropic displacement field [19]. The edge dislocation of $b = 1/2[\bar{1}\bar{1}0]$ is introduced by removing two [110] half planes. The 60 degree mixed dislocation of $b = 1/2[0\bar{1}1]$ is introduced by introducing an $1/4[\bar{1}\bar{1}0]$ screw dislocation in y direction and removing three $[\bar{1}\bar{1}2]$ half planes ($\frac{1}{2}[0\bar{1}1] = \frac{1}{4}[\bar{1}\bar{1}0] + \frac{1}{4}[\bar{1}\bar{1}2]$).

To generate an SFT, a triangular vacancy platelet of 153 vacancies is inserted to the system, which forms an SFT with edge length of 4.6 nm, about twice as large as the experimentally observed value of 2.5 ± 0.5 nm [8]. The snapshot of the simulation cell containing the 4.6 nm SFT and a screw dislocation is shown in Fig. 1.

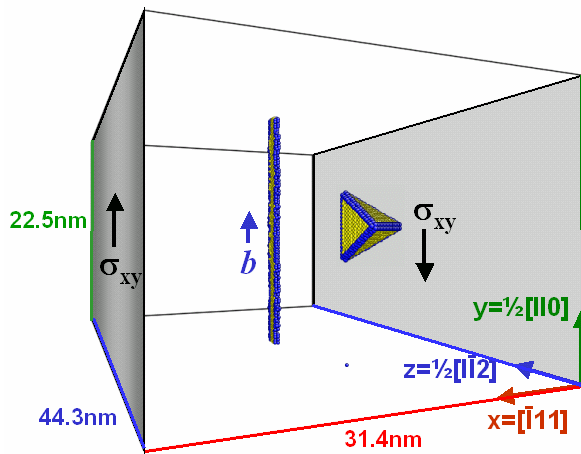


Fig. 1. The interaction geometry between a screw dislocation and an SFT.

Periodic boundary conditions are used in the y and z directions, while the x direction is a free surface, subject to an applied shear surface traction. In the case of a screw dislocation, the periodic boundary condition in the z direction is modified by shifting atomic positions by $\pm b/2$ in the y direction to ensure the continuity of the [110] plane across the periodic boundary in the z direction, following the work of Rodney [20]. In the case of a mixed dislocation, the amount of shift in the y direction is set to $\pm b/4$. The simulation cell was equilibrated for 50 ps at $T = 100$ K using an NVE ensemble. Following equilibration, a shear stress of 300 MPa is applied to the system by adding forces parallel to the corresponding Burger's vector direction to the atoms on the free surface x.

The visualization of the interaction process of the SFT and dislocation are performed using the common neighbor analysis [19]. This method identifies the local atomic structure as a sequence of three integers (ijk) for each first nearest neighbor pairs (root pair). The first integer (i) is the number of nearest neighbor atoms shared in common by the root pair. The second (j) is the number of nearest neighbor bonds among the common neighbors. The third integer (k) is the length of continuous nearest neighbor bonds among the common neighbors. For example, the FCC structure gives only 421, while the hexagonal closed packed (HCP) structure gives equal amounts of 421 and 422. Using this information, the atoms are color coded to represent different local order. The yellow atoms are atoms in HCP structure, thus corresponding to stacking faults, and blue atoms are neither FCC nor HCP, corresponding to dislocation or stair-rod partial dislocation cores.

Results and Discussion

For the interaction geometry used in this study, the resulting SFT structures immediately after the interaction with screw, mixed and edge dislocations are almost identical, even though the sequence of events during the interaction processes are different. As shown in Fig. 2, the SFT is effectively decomposed into a smaller perfect SFT and a truncated base regardless of the character of the dislocation with which it interacted. The truncated base is a sessile defect, composed of four Shockley and six stair-rod partial dislocations.

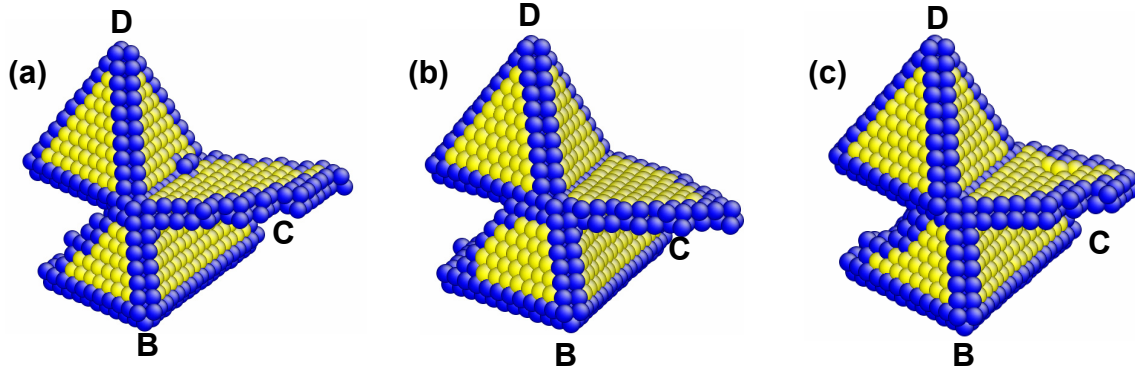


Fig. 2. The structure of SFT immediately after the detachment of trailing partial (δA) when the gliding dislocation is (a) Screw dislocation ($b = BA$), (b) Edge dislocation ($b = BA$), (c) Mixed dislocation ($b = CA$). The δA trailing partial detached by an Orowan-like mechanism, leaving δA segment on the SFT.

Shortly after the detachment of the trailing partial, which occurs by an Orowan-like mechanism, additional dislocation reactions occur between the small perfect SFT and the truncated base, resulting in transformation to a sheared SFT structure containing ledges. These structures are shown in Fig. 3. The ledges shown in (a) and (c) are consistent with the anticipated interstitial (I) and vacancy (V)-ledges formed as a result of shear of the SFT [22]. Notably, the ledges are often unstable and can self-heal through dislocation glide reactions, as expected from the relatively high ledge energies.

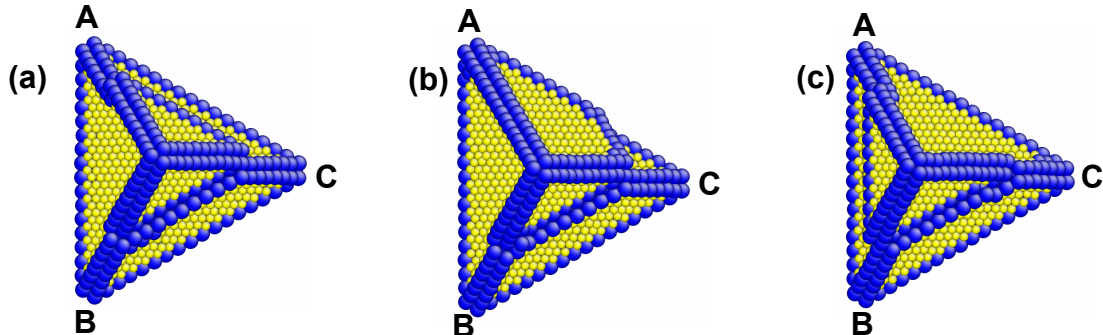


Fig. 3. The structure of SFT 5ps after the detachment of trailing partial (δA) when the gliding dislocation is (a) Screw dislocation ($b = BA$), (b) Edge dislocation ($b = BA$), (c) Mixed dislocation ($b = CA$). Note that along the burgers vector, no ledges are formed on the sheared SFT surface.

The interaction mechanisms observed in the MD simulations are summarized as below:

Screw dislocation (BA) interacting with an SFT (Fig. 4)

The dissociated partial dislocations ($B\delta$ and δA) of the screw dislocation ($\vec{b} = BA$) intersect with the SFT as they glide on the (d)-plane. Initially, the segment bounded by the SFT constricts on the inclined (c) surface of the SFT. Subsequently, the screw dislocation re-dissociates on the (c)-plane as $B\gamma$ and γA , following cross slip (Fig. 4(a)). Immediately thereafter, γA moves towards the base, eliminating the stacking fault on the lower portion of the SFT. When γA meets the stair-rod $\gamma\beta$ on the AD edge and the $\delta\gamma$ stair-rod on the AB edge, it forms βA and δA Shockley partials on the (b) and (d)-planes, respectively. These two Shockley partials move on the (b) and (d)-planes, eliminating the stacking faults of the SFT on the (b) and (d)-planes (Fig. 4(b)).

As a result of the applied shear stress, the screw partials on the (d)-plane outside of the SFT bow around the SFT. Around the constriction point E, $B\delta$ glides inside the SFT and forms $\delta\gamma$ on the (c)-plane, which is an edge of a smaller SFT. At the same time, the trailing δA partial glides along with $B\delta$ and forms $\delta\beta$ by a reaction with βA ($\delta A + A\gamma \rightarrow \delta\beta$) on the (b)-plane, which is also an edge of a smaller SFT (Fig. 4(c)). At the constriction point F, $B\alpha$ is formed on (a)-plane and reacts with the leading $B\delta$ partial, forming $\delta\alpha$ stair rod dipole. The trailing δA is detached from the truncated base by an Orowan-like mechanism, thus leaving the δA Shockley partial attached to the $\delta\alpha$ stair rod of the truncated base.

Edge dislocation (BA) interacting with an SFT (Fig. 5)

The leading $B\delta$ partial is constricted on the (b)-face of the SFT as the dissociated partials move toward the SFT (Fig 5a). Upon continuous applied shear stress, the stair-rod partials of SFT around the point A dissociate into Shockley partials by a reverse Silcox-Hirsch process. As the SFT opens up starting from point A, the $B\delta$ glides inside of the SFT while dragging the γA and βA Shockley partials (Fig 5b). Then, the trailing partial δA moves towards the SFT and reacts with the Shockley partials γA and βA , forming stair-rod partials $\delta\beta$ on (b)-face and $\delta\gamma$ on (c)-plane, respectively. The resulting stair-rod partials are edges of the smaller SFT.

As both partials constrict on the (a)-face of the SFT, $B\alpha$ is formed on (a)-plane and reacts with the leading $B\delta$ partial, forming a $\delta\alpha$ stair rod dipole. The trailing δA detaches from the truncated base by an Orowan-like mechanism, thus leaving a δA Shockley partial attached to the $\delta\alpha$ stair rod of the truncated base.

Mixed dislocation (CA) interacting with an SFT (Fig. 6)

The dissociated partial dislocations ($C\delta$ and δA) of the mixed dislocation ($\vec{b} = CA$) intersect with the (c)-face of the SFT as they glide on the (d)-plane. They first constrict on the (c)-face of the SFT, then dissociate into Shockley partials $C\delta$ and γA and the stair-rod partial $\delta\gamma$. $\delta\gamma$ forms an edge of the small SFT, while the γA starts to move toward the base of the SFT, eliminating the stacking faults and edges around the point A. The reaction of γA is similar to that observed for the screw dislocation.

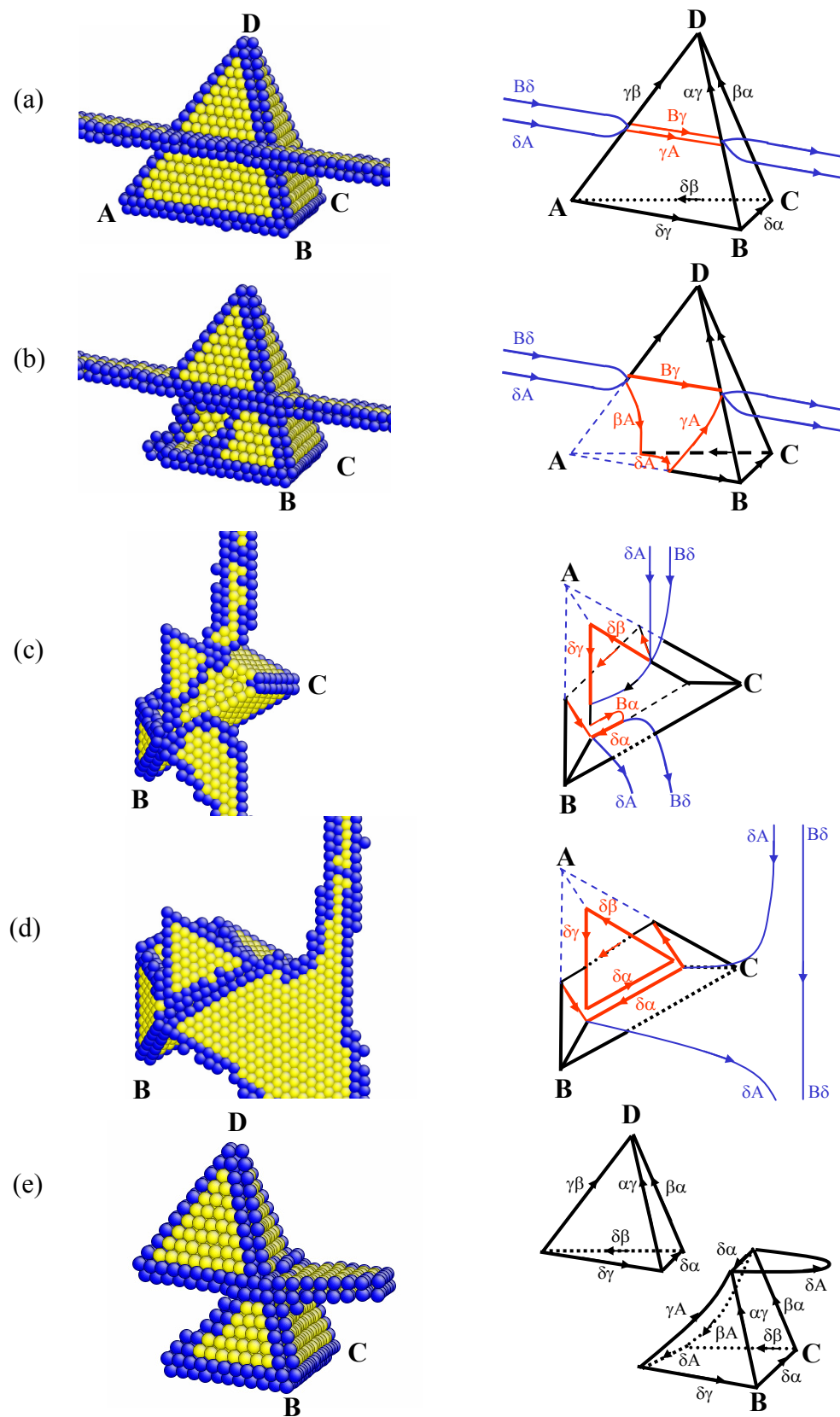


Fig. 4. Screw dislocation ($b = BA$) passing the SFT at applied shear stress 300 MPa.

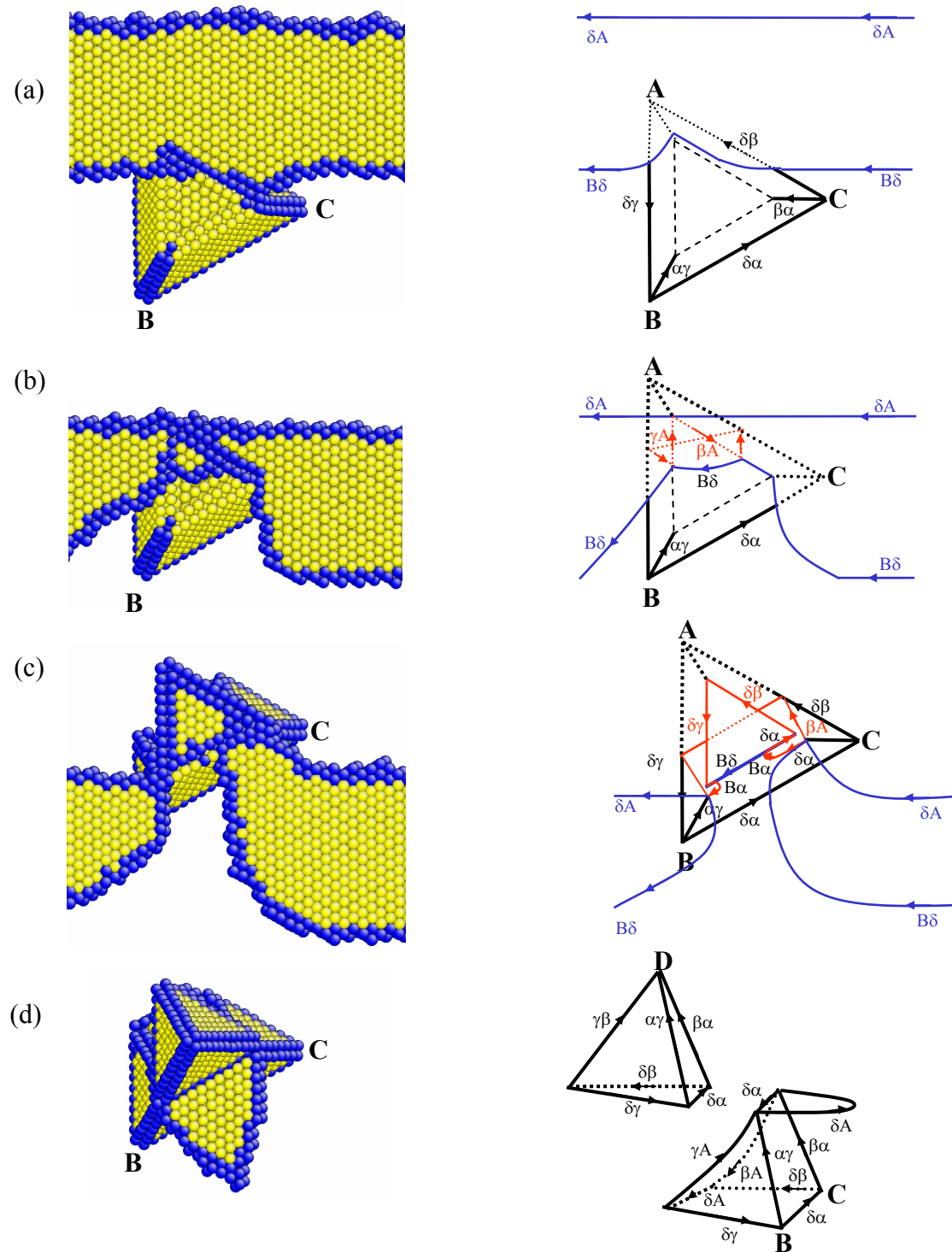


Fig. 5. Edge dislocation ($b = BA$) passing the SFT at applied shear stress 300 MPa.

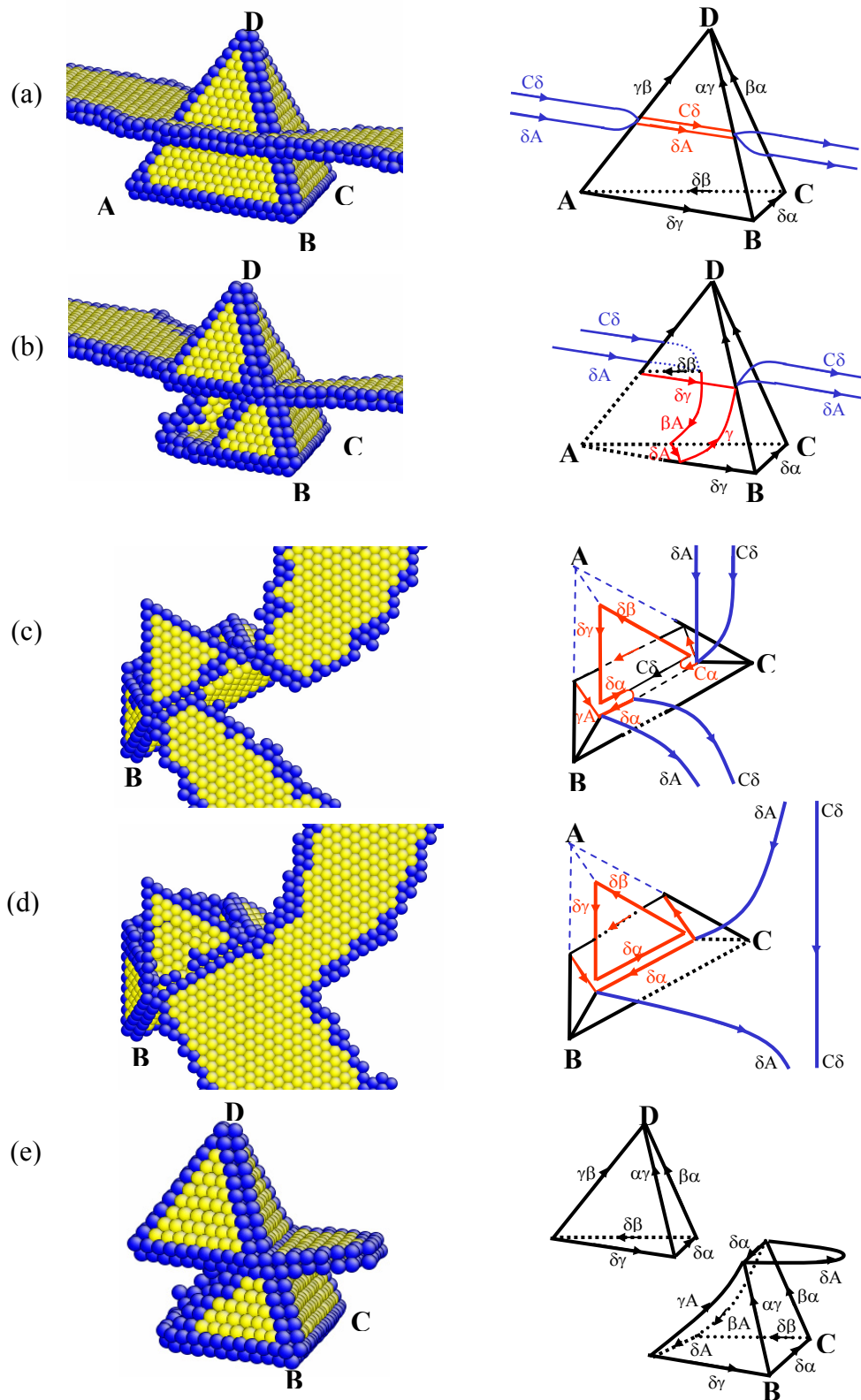


Fig. 6. 60 degree mixed dislocation ($b=CA$) passing the SFT at applied shear stress 300MPa.

As the leading $C\delta$ cuts through the SFT, the trailing δA forms $\delta\beta$ on the (b)-face of the SFT, producing an edge of the small SFT. When both partials constrict on the (a)-plane, $C\alpha$ is formed. $C\alpha$ reacts with $C\delta$, forming a $\delta\alpha$ stair-rod dipole. Identical to the previous two cases, the trailing δA detaches from the truncated base by an Orowan-like mechanism, thus leaving a δA Shockley partial attached to the $\delta\alpha$ stair rod of the truncated base.

Conclusions

The interaction mechanisms between an SFT and gliding screw, edge and mixed dislocations are studied using molecular dynamics simulation methods. Each type of dislocation exhibits a different interaction behavior upon initial contact with the SFT. A screw dislocation cross-slips onto the inclined surface of the SFT. One of the cross-slipped Shockley partials moves toward the base of the SFT, thereby partially eliminating the stacking fault of the SFT. An edge dislocation induces SFT instability and partial collapse by a reverse Silcox-Hirsch process upon contact. A mixed dislocation dissociates into Shockley partials and a stair rod partial dislocation on the inclined face of the SFT. However, in all cases, the dislocation bypasses the SFT prior to complete absorption or annihilation of the defect. The trailing partial detaches from the truncated base by an Orowan-like mechanism, independent of dislocation character. The detailed SFT-dislocation interactions are explained in terms of the governing partial dislocation reactions. Regardless of the dislocation character, an SFT is transformed to a smaller perfect SFT and a truncated base as the dislocation passes through the SFT, which then finally transforms into a sheared SFT with I and V-ledges.

Acknowledgements

This work has been supported by the Office of Fusion Energy Sciences, U.S. Department of Energy, under Grant DE-FG02-04ER54750.

References

- [1] M. Victoria, N. Baluc, C. Bailat, Y. Dai, M. I. Lupo, R. Schaublin, and B. N. Singh, The microstructure and associated tensile properties of irradiated FCC and BCC metals, *J. Nucl. Mater.* 276 (2000) 114–122.
- [2] R. S. Averback and T. D. de la Rubia, Displacement damage in irradiated metals and semiconductors, *Solid State Physics—Advances In Research and Applications* 51 (1998) 281–402.
- [3] D. Rodney, Atomic-scale modeling of clear band formation in FCC metals, *Nucl. Instrum. Methods Phys. Res. Sect. B: Beam Interact. Mater.* 228 (2005) 100–110 (Special Issue SI).
- [4] B. N. Singh and S. J. Zinkle, Defect accumulation in pure FCC metals in the transient regime—A review, *J. Nucl. Mater.* 206 (2-3) (1993) 212–229.
- [5] J. Silcox and P. B. Hirsch, Direct observations of defects in quenched gold, *Philos. Mag.* 4 (37) (1959) 72–89.
- [6] B. D. Wirth, V. Bulatov, and T. D. de la Rubia, Atomistic simulation of stacking fault tetrahedra formation in Cu, *J. Nucl. Mater.* 283 (2000) 773–777 (Part B Ded).
- [7] Y. N. Osetsky, D. J. Bacaon, B. N. Singh, and B. Wirth, Atomistic study of the generation, interaction, accumulation, and annihilation of cascade-induced defect clusters, *J. Nucl. Mater.* 307 (2002) 852–861 (Part B).
- [8] B. N. Singh and S. J. Zinkle, Defect accumulation in pure FCC metals in the transient regime—A review, *J. Nucl. Mater.* 206 (2-3) (1993) 212–229.
- [9] B. D. Wirth, W. Bulatov, and T. D. de la Rubia, Dislocation-stacking fault tetrahedron interactions in Cu, *J. Eng. Mater. Technol. (Trans. ASME)* 124 (3) (2002) 329–334.
- [10] Y. N. Osetsky, R. E. Stoller, and Y. Matsukawa, Dislocation-stacking fault tetrahedron interaction: What can we learn from atomic-scale modeling, *J. Nucl. Mater.* 329 (2004) 1228–1232 (Part B).
- [11] J. S. Robach, I. M. Robertson, B. D. Wirth, and A. Arsenlis, In-situ transmission electron microscopy observations and molecular dynamics simulations of dislocation-defect interactions in ion-irradiated copper, *Philos. Mag.* 83 (8) (2003) 955–967.

- [12] H. Kimura and R. Maddin, Lattice defects in quenched metals, in R. Cotterill (ed.), Proceedings of an International Conference, Argonne National Laboratory, June 15–17, 1964 (Academic Press, New York, 1965) 319.
- [13] E. Johnson and P. B. Hirsch, Insitu straining In the HVEM of neutron-irradiated copper-crystals, *Philos. Mag. A–Phys. Cond. Matter Struc. Def. Mech. Prop.* 43 (1) (1981) 157–170.
- [14] Y. Matsukawa and S. J. Zinkle, Dynamic observation of the collapse process of a stacking fault tetrahedron by moving dislocations, *J. Nucl. Mater.* 329–333 (2004) 919–923 (Part B).
- [15] T. D. De La Rubia and M. W. Guinan, Progress in the development of a molecular-dynamics code for high-energy cascade studies, *J. Nucl. Mater.* 174 (2-3) (1990) 151–157.
- [16] Y. Mishin et al., Structural stability and lattice defects in copper: Ab initio, tight-binding, and embedded-atom calculations, *Phys. Rev. B* 63 (22) (2001) Art. No. 224106.
- [17] G. Simons and H. Wang, Single Crystal Elastic Constants and Calculated Aggregate Properties, MIT Press, Cambridge, Mass. (1977).
- [18] C. B. Carter and I. L. F. Ray, *Philos. Mag.* 35 (1977) 189.
- [19] J. Weertman and J. R. Weertman, Elementary Dislocation Theory, Oxford University Press (1992).
- [20] D. Rodney, Molecular dynamics simulation of screw dislocations interacting with interstitial frank loops in a model FCC crystal, *Acta Mater.* 52 (3) (2004) 607–614.
- [21] A. S. Clarke and H. Jonsson, Structural-changes accompanying densification of random hard-sphere packings, *Phys. Rev. E* 47 (6) (1993) 3975–3984.
- [22] D. Kuhlmann, Growth and annealing of stacking fault tetrahedra, *Acta Metall.* 13 (3) (1965) 257.